

Coupled chemical and mechanical processes in concrete structures with respect to aging

Friedhelm Cramer^{*}, Ursula Kowalsky^a and Dieter Dinkler^b

Institute for Structural Analysis, TU Braunschweig, Beethovenstraße 52, 38106 Braunschweig, Germany

(Received February 11, 2014, Revised March 15, 2014, Accepted March 20, 2014)

Abstract. Accurate prognoses of the durability of concrete structures require a detailed description of the continuously running aging processes and a consideration of the complete load history. Therefore, in the framework of continuous porous media mechanics a model is developed, which allows a detailed analysis of the most important aging processes of concrete as well as a flexible coupling of different processes. An overview of the prediction model and the balance equations is given. The material dependent model equations, the consequences of coupling different processes and the solution scheme are discussed. In two case studies the aging of concrete due to hydration and chloride penetration are presented, which illustrate the capabilities and the characteristics of the developed model.

Keywords: THCM modeling; porous media; aging of concrete; degradation

1. Introduction

Concrete is one of the most common materials because concrete structures are usually durable and maintenance-free. But the material behavior of concrete is changing over the life cycle, and varies depending on composition, environmental and different other influences. The modeling of the material behavior and its evolution over the life cycle is very complex, since models are needed for different chemical and mechanical processes operating on different spatial and temporal scales. Often changes in time of the material behavior are described by the term degradation, e.g., Baroghel-Bouny *et al.* (2011), Bangert *et al.* (2004). The main idea of this contribution is the assumption that all changes of the physical and chemical properties of concrete have to be described as aging processes, which are coupled on different scales in space and time.

The individual aging mechanisms are very complex and still subject of current research. Experimental studies of the aging mechanism are very time-consuming because of low process velocities. Therefore, numerical models are developed, which allow a systematic investigation of aging processes and an identification of the relevant influences and parameters, see Steffens *et al.* (2002), Baroghel-Bouny *et al.* (1999), Gawin *et al.* (2003) and Ostermann (2011).

^{*}Corresponding author, Dipl.-Ing., E-mail: f.cramer@tu-bs.de

^a Dr.-Ing., E-mail: u.kowalsky@tu-bs.de

^b Professor Dr.-Ing., E-mail: d.dinkler@tu-bs.de

Here, a numerical model is introduced, which allows the description of the most important aging processes in concrete via a monolithic algorithm. Therewith, the model can be used for numerical analysis of the whole life cycle. Furthermore, the effect of each process on the durability of the structure can be evaluated separately.

The advantage of the model is the possibility of coupling different aging mechanism. On the one hand coupling of processes, which proceed at the same time scale is possible. On the other hand processes may be coupled consecutively in time. The coupling allows the predictive analysis of concrete constructions over the life cycle. Moreover the results of regular inspections or results of monitoring may be introduced to the model anytime. An update of the model parameters as well as of the external loads is possible. Hence the prediction may be improved substantially.

The approach is used to analyze the influence of the hydration process on the transport behavior of concrete during the life cycle. The hydration process depends on different parameters, which governs the development of resistance, humidity and heat etc. A deficient core prevents full hydration of the concrete and causes degradation of resistance due to porosity and water concentration. Here, the transport of chloride is used as an example.

2. Prediction model

This work aims for a numerical model that allows the description of the main processes in reinforced concrete structures during their life cycle. This requires a formal treatment and a general description of the different processes. Therefore the presented model comprises three parts: the principal variables, the principal processes to be described and the required material models, see Fig. 1. The principal variables characterize the general state of the construction during the life cycle. Most important variables are the deformation, relative humidity, temperature, concentration of substances dissolved in water or as part of the gas phase and the degree of hydration. The principal processes describe the development of the principal variables in space and time. Transport, reaction and deformation behavior could be identified as the most significant principal processes. Different principal processes may be investigated additionally according to external hazards during the life cycle.

In addition to the formal treatment constitutive models dependent on specific phenomena and materials are needed and presented in the following section. The deformation is the most determining process for the assessment of the structural response. The corresponding mechanical model characterizes the stress-deformation behavior. Different material models for the description of time dependent viscous material behavior or multi surface plasticity models are incorporated.

The description of the degradation of the structure due to extreme environmental conditions requires the consideration of water and heat transport, which are described by the relative humidity and temperature as principle variables. Additionally the transport of substances like chloride or carbonate is taken into account by means of their concentration in pore water und gas, because their influence on the chemical composition of concrete.

Beside the transport and the deformation the sum of the chemical reactions considered is the third principal process incorporated. A lot of chemical reactions arise in the cement paste for example due to the hydration of aging concrete or the dehydration in concrete under high temperatures or chemical attacks. The reaction kinetics have to be formulated for each process. Here, the hydration process, dehydration, chloride binding and carbonation are considered.

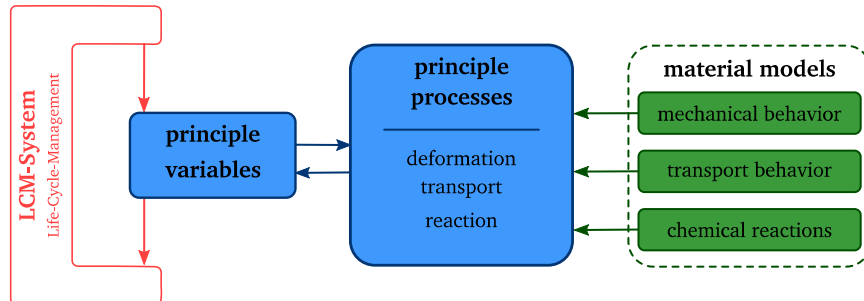


Fig. 1 Prediction model

The presented model allows the numerical analysis of different coupled processes during the life cycle of concrete structures, for example of hygro-thermal transport, deformation and reaction regarding hydration and chloride binding.

The sequence of the prediction model is subdivided into three steps. In the first step the relevant principle variables are selected and defined by initial conditions. Afterwards principal processes are activated for each principal input variable and combined with corresponding material models. Finally the development of the principal variables can be computed. The formal procedure is displayed in Fig. 1.

The formal framework introduced here allows a simple integration of the presented model into an existing global Life-Cycle-Management system (LCM), which is shown in Fig. 1, too. Thereby, the principle variables serve as an interface. All principle variables are stored in the LCM system. At the beginning of an analysis the relevant principle variables are selected from the LCM system and sent to the prediction model, which activates the corresponding principle processes and material models and computes the evolution of the principle variables. At the end the updated principal variables are given back to the LCM.

3. Balance equations

Concrete is a heterogeneous material, which consists of the three main constituents cement, water and aggregates. During the hydration process, water and cement reacts and the hardened cement paste occurs. After hydration process has been completed there exist pores in the hardened cement paste, which are partially filled with water or gas. The size and the structure of the pores significantly influence the aging behavior of the concrete and therefore have to be considered in the model.

The description of the principle processes in concrete, which are introduced in Section 2, is developed in the context of the theory of porous media. Therefore the governing equations have to be formulated for the three phases solid, liquid and gas. A short overview of the balance equations is presented in this section.

Transport may be described generally by the conservation of mass for every component π of the three phases α with

$$\frac{\partial}{\partial t} (n_\alpha \tilde{\rho}_\alpha \omega_{\pi\alpha}) + \nabla \cdot (n_\alpha \tilde{\rho}_\alpha \omega_{\pi\alpha} \mathbf{v}_\alpha) + \nabla \cdot (n_\alpha \tilde{\rho}_\alpha \omega_{\pi\alpha} \mathbf{v}_{\pi\alpha}) = \sum_{\beta \in J_{c\alpha}} \dot{m}_{\beta \rightarrow \alpha} + n_\alpha r_{\pi\alpha} \quad (1)$$

where n_α characterizes the particular volume fraction of α . The first term describes the changes in the local mass depending on the changes in volume fraction, intrinsic density or the concentration ω of the regarded component π in the phase α . The advective transport depends on the phase velocity \mathbf{v}_α . Additionally diffusion phenomena may occur in phases with more than one component, which is described by the diffusive velocity $\mathbf{v}_{\pi\alpha}$ of component π in phase α . The right hand side term in Eq. (1) considers the exchange of masses between the phases β and α and possible reactions between the components π of phase α .

The transport of energy takes place in the hardened cement paste and the aggregates as well as in the pore water and pore gas. Due to assumption of thermodynamically equilibrium of all phases, the energy transport follows

$$C_{p,c} \frac{\partial T}{\partial t} + \sum c_{p\alpha} \mathbf{q}_\alpha \cdot \nabla T - \nabla \cdot \mathbf{q}_e + J_t \Delta h_{vap} = r_e \quad (2)$$

with the effective heat capacity of the porous material $C_{p,c}$, the sum of the convective transport parts, the energy flux \mathbf{q}_e and the energy from vaporization of water. Sources due to chemical reactions are balanced on the right hand side in r_e .

The reaction processes are indirectly involved in the governing equations for energy and mass. Any chemical reaction leads to a consumption of reactant and to the formation of new products. Both, reactant and new products, are introduced into the mass balances by additionally source terms in Eq. (1). The enthalpies of the reactions are stored in Eq. (2).

The deformation process is described for all phases by means of the balance of linear momentum, which usually has to be formulated for all phases. Taken into account, that the acceleration and the velocity of the deformation processes are negligible small, and that the sum of forces due to interactions between the phases is zero, the linear momentum for the multi phase material follows

$$\nabla \cdot \boldsymbol{\sigma} + \rho_c \mathbf{g} = \mathbf{0} \quad (3)$$

with the macroscopic Cauchy stress $\boldsymbol{\sigma}$ and the average density of concrete ρ_c . The focus of this contribution will lie on the investigation of the influence of the hydration on the chloride penetration process to assess the risk of corrosion. Therefore, the balance of linear momentum and the balance equations for water and vapor, dry air, energy, chloride concentration and carbon dioxide concentration have to be considered. Here, the evolution of the variables \mathbf{u} , φ , T , p_a , $\omega_{\gamma w}$ and $\omega_{\kappa a}$ is investigated.

4. Modelling of aging processes

The modeling of aging processes in concrete requires, beside the balance equations from Section 3, additional material models to describe the mechanical and transport behavior and the characteristics of the running chemical reactions. The material models are the third part of the presented prediction model and assembled in this section.

4.1 Reaction processes in the cement paste

The aging of concrete due to chemical reactions happens in the cement paste between components of the cement paste, additional substances, which have penetrated from the ambience, and between the substances themselves. Generally, the reaction processes are described by a stoichiometry. Modeling of the chemical processes in context of the presented framework requires a transfer of the reaction equation into a mathematical rate description.

Formally, a chemical process may be described by the degree of reaction Γ_{chem} , which characterizes the reaction state and is defined between 0 and 1. In case of $\Gamma_{chem} = 0$ the reaction has not been started, whereas $\Gamma_{chem} = 1$ characterizes a fully completed reaction. The reaction rate is defined by

$$\dot{\Gamma}_{chem} = g(\Gamma_{chem}) \cdot f_T \cdot f_H \quad (4)$$

where $g(\Gamma_{chem})$ is the process rate. In general, g depends on Γ_{chem} . Furthermore, the concentration of reactants and products may be taken into account by g . Additional influences on the process rate may be considered in Eq. (4) by additional arguments. In the presented case, the influences of temperature and relative humidity are regarded by f_T and f_H .

4.1.1 Cement hydration

The hydration is a spontaneous reaction, which starts by adding water to the cement. The reaction leads to the formation of the so-called hydrate phases and the structure of the hardened cement paste, which provide the strength of the composite material. The hydration stops when no more reactants are available.

A detailed description of the reactions of the different cement components and the building of the different hydrate phases is practically impossible and not necessary for the description of the macroscopic behavior of the structure. Therefore the chemical process is described as a global exothermic, thermal activated reaction of the cement and the pore water. According to Eq. (4), the degree of the hydration reaction is defined by

$$\dot{\Gamma}_{hyd} = g_m(\Gamma_{hyd}) \cdot f_T \cdot f_H \quad (5)$$

where $g_m(\Gamma_{hyd})$ is the process rate and f_T and f_H consider the influence from climate conditions. The first one takes into account the temperature conditions, which may lead to an acceleration of the reaction. The second one describes the deceleration of the process by lower moisture content. In practice, the degree of hydration m is usually used instead of the degree of the chemical reaction Γ_{hyd} to characterize the material behavior. It is defined by

$$\dot{m} = \dot{\Gamma}_{hyd} \cdot m_\infty \quad (6)$$

with the theoretical final degree of hydration $m_\infty < 1$, which can be estimated by the proposal from Pantazopoulou and Mills (1995). The effects of the hydration process on the mechanical and transport behavior will be explained in Section 4.2.

4.1.2 Chloride binding

Chloride ions in concrete are undesired, because they may destroy the passive layer of the

reinforcement, also at very high existing basicity. The subsequent onset of corrosion may affect the bearing capacity and leads to damage of the concrete due to increased volume of the corrosion products.

There are two kinds of chlorides in concrete. Either the chlorides are bound in the cement paste or on the pores surface, or they are available as free ions in the pore water. Only the last form acts strong corrosively. Therefore a differentiation between free and bound chlorides is necessary. Here, the Langmuir isotherm is used to relate the dissolved chloride γ to the bounded chloride γ_r . The degree of the binding reaction follows

$$\dot{\Gamma}_\gamma = \frac{\partial}{\partial t} \left(\frac{k_c \cdot \gamma}{1 + k_c \cdot \gamma} \right) \cdot f_{KG} \cdot f_n, \quad (7)$$

where the parameter k_c is determined by adaptation to experimental results. The reduction of the pH value due to carbonation and the associated decrease in the binding capacity of the cement is considered in the Eq. (7) by f_{KG} . Additionally the influence of the porosity is taken into account with f_n , as it is proposed for example by Derluyn (2014). The amount of bound chloride γ_r , which is needed for the chloride balance Eq. (1) can be calculated by

$$\dot{\gamma}_r = \dot{\Gamma}_\gamma \cdot \gamma_{r,max} \quad (8)$$

where $\gamma_{r,max}$ is the maximal binding capacity of the material.

4.1.3 Carbonation

The carbonation process describes in general the reaction of carbon dioxide with different phases of the cement paste. Carbon dioxide reaches thereby almost exclusively gaseous from the ambience in the pore space. The carbonation process is not directly aggressive to the concrete and even has some positive aging aspects. Depending on the cement type the carbonation leads to a decrease of porosity and therewith a deceleration of transport of water and substances.

Here, the carbonation reaction of carbon dioxide and calcium hydroxide is taken into account. The reaction can be subdivided into two parts. In the first step the carbon dioxide, diffused from the surface into the pore space, is dissolved in the pore water. Then, the carbon dioxide reacts with dissolved components of the cement paste to calcium carbonate. According to Eq. (4) the mathematical formulation of the evolution of the carbonation process follows

$$\dot{\Gamma}_\kappa = g_\kappa(\Gamma_\kappa) \cdot f_H \cdot f_K \quad (9)$$

with the reaction rate $g(\Gamma_\kappa)$ and the two arguments f_H and f_K which take into account the influence of the concentration of water f_H and calcium hydroxide f_K on the reaction velocity. The definition of the reaction rate is based on the Arrhenius equation and follows

$$g_\kappa(\Gamma_\kappa) = \alpha \cdot A \cdot \exp\left(\frac{E_a}{R \cdot T}\right) \cdot \frac{(1 - \Gamma_\kappa)}{\kappa_{r,max}}. \quad (10)$$

The parameters of the Arrhenius function α , A and E_a are taken from Saetta *et al.* (1993). The maximum of carbon dioxide, which may react with the cement past is denoted by $\kappa_{r,max}$ and depends on the calcium oxide concentration of the cement. A detailed description of the carbonation model is given in Steffens (2002). The source term for carbon dioxide balance, see Eq. (1), is defined analogously to Eq. (8) with κ_r , Γ_κ and $\kappa_{r,max}$. Furthermore, the water, which is

released during the carbonation process, leads to an additional source term for the water balance.

4.2 Transport processes in the porous material

Transport processes in porous materials are significantly depending on the structure of the pore space, the size of the pores and the saturation with water or gas. Therefore, models describing the pore structure and the saturation are needed and presented in order to describe the transport processes accurately.

4.2.1 Porosity and saturation

The pore structure of the concrete is subjected to permanent aging processes during the life-cycle because the running reaction processes lead to changes in the hardened cement paste structure. The highest change in pore structure occurs during the hydration process. Jensen *et al.* (2001) develop a model to describe the evolution of porosity during the hydration process, which is used in this work. In the model the porosity n depends on the concrete composition, the maximum degree of hydration and the actually degree of hydration.

The effects of further chemical reactions are considered additionally subjected to the respective degree of reaction. Therewith the time-varying porosity follows

$$n = n_0(m) - A_n^{\text{Cl}_r} \cdot \Gamma_\gamma - A_n^{\text{CO}_2,r} \cdot \Gamma_\kappa, \quad (11)$$

where the additional parameters are to be determined experimentally.

In the porous concrete on the one hand water is presented as chemical bounded water in the cement paste and on the other hand as physical adsorbed water or due to capillary condensation in the pore space. Only the latter is relevant for the discussed transport and reaction processes.

There are a lot of different models for the description of pore saturation available in the literature. Many authors use the capillary pressure saturation relationship of van Genuchten. Here, a modified version of the saturation model proposed by Tacke (2002) is employed. Tacke describe the two saturation phenomena physical sorption and capillary condensation separately and add them to the total saturation. Depending on the relative humidity φ the saturation follows

$$S_w = -\frac{w_m}{w_s} \cdot \ln \left(\frac{RT \ln(\varphi)}{\Delta\mu_0} + C \right) + \left(1 - p \cdot \frac{w_m}{w_s} \right) \cdot f_{kd} \quad \text{with} \quad 0 \leq f_{kd} \leq 1. \quad (12)$$

The parameters w_s and w_m describe the water content for the saturated material and the water content of the monolayer and depend on the concrete composition and the degree of hydration. Furthermore $\Delta\mu_0$ corresponds to the start potential of the onset of adsorption and C the onset of condensation at high relative humidity.

The second part describes the capillary condensation, which starts at relative humidity larger than 40%. Here, f_{kd} is the capillary filling factor, which describes the condensate formation in the remaining pore space upto water saturation. All parameters are discussed in detail in Tacke (2002).

A salt concentration in the pore water leads to a change in the hygroscopic properties of the solution. The hygroscopic effect of the salt starts, when the relative humidity exceeds φ_{hygr} and more water molecules are dissolved, which further dilute the solution and increase the water content. Full saturation is reached for even $\varphi_{sol} < 100\%$ depending on the salt content. The water vapor pressure of the solution at a given temperature is less than the comparable via pure water.

Here, the hygroscopic effect is taken into account with the Raoult law, which replaces Eq. (12).

The function is implemented with a smooth rounding at φ_{hygr} on the left side and for full saturation on the right side to get a continuously proceeding function. Fig. 2 shows the course of the saturation for different salt contents. In case of sodium chloride the hygroscopic effect starts above $\varphi_{hygr} = 75\%$.

4.2.2 Transport

The transport processes in porous materials may be divided in advective flow of water and gas and in transport caused by diffusion. The first one is described for the liquid and the gas phase by Darcy's law

$$\mathbf{q}_\alpha = \tilde{\rho}_\alpha^\pi \frac{\mathbf{k} k_{r\alpha}}{\mu_\alpha} (-\nabla p_\alpha + \tilde{\rho}_\alpha \mathbf{g}) \quad \text{with} \quad \alpha = w, g, \quad (13)$$

where \mathbf{k} is the intrinsic permeability, $k_{r\alpha}$ the relative permeability and μ_α the dynamic viscosity of the current phase α . The intrinsic permeability quantifies the transport behavior in porous media and considers the influences of changes in pore space due to chemical reactions, pore pressure and mechanical damage like cracks. Therefore a product approach proposed by Gawin *et al.* (2003) is used and the intrinsic permeability is defined by

$$\mathbf{k} = k_0 \cdot k_{chem}(n) \cdot k_p(p_g, n) \cdot k_D \cdot \mathbf{I}, \quad (14)$$

with k_0 as initial permeability. Ostermann (2011) gives a detailed overview of the definition of each part of Eq. (14). The second transport part describes the diffusion of component π through phase α due to the concentration gradient of component π . Here Fick's law

$$\mathbf{q}_\alpha^\pi = -\tilde{\rho}_\alpha D_\alpha^\pi \nabla \omega_\alpha^\pi \quad (15)$$

is used in the general form for the binary diffusion of water vapor and dry air. In Eq. (15) D_α^π describes the effective diffusivity tensor which is defined by

$$D_\alpha^\pi = D_{\alpha,0}^\pi f_\alpha^s \frac{p_0}{p_g} \left(\frac{T}{T_0} \right)^{1.81} k_D \mathbf{I}. \quad (16)$$

Here, f_α^s is a structural factor to take into account the tortuosity, the porosity and the saturation. The diffusion of the carbon dioxide in dry air is described by Eq. (15), too, but the interactions between the diffusion processes are neglected. This is justified because on the one hand the concentration of carbon dioxide in dry air is about 0.054 m-% and therewith the influence on the diffusion of dry air and vapor is very small. On the other hand the velocity of carbon dioxide diffusion is very slow in comparison to dry air or water vapor, because the carbon dioxide reacts to carbonate in the parallel reaction process.

Salt ions penetrate only in dissolved form in the porous concrete. In addition to Eq. (13) the ions may diffuse into the solution, which is described by Eq. (15). However, the different diffusion rates of the sodium and chloride ions remain unconsidered since only the amount of corrosive chloride ions is of interest.

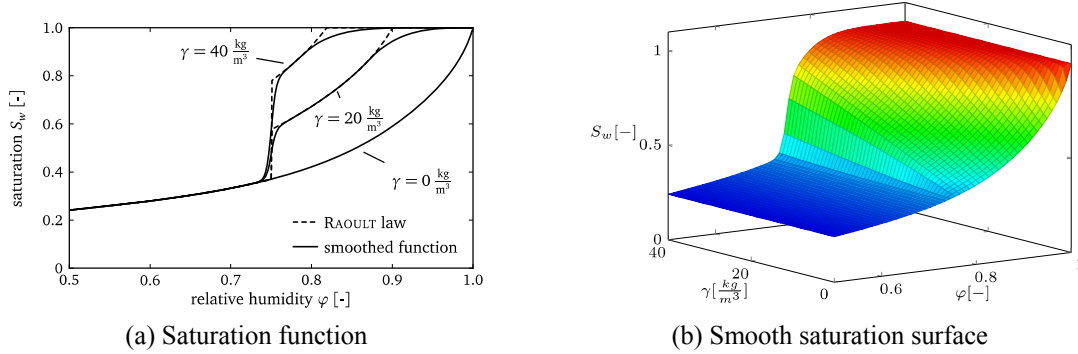


Fig. 2 Saturation function with and without chloride

4.3 Mechanical behavior

4.3.1 Effective stress concept

Additionally to the running reaction processes the aging of concrete may be a result of mechanical processes that may occur independently of outer loads. For example, changes in the concentration of the pore fluids due to the principle processes transport and reaction, lead to a change of the pore pressure in porous materials, which interacts via the pore walls with the solid phase.

The influence of pore pressure p_s on the deformation processes may be considered by the concept of effective stress. The effective stress

$$\sigma' = \sigma + \alpha p_s I \quad (17)$$

is defined as the sum of the total stress σ and the pressure of the solid phase p_s and thus takes into account both, external loads and internal pore pressure. In Eq. (17) α is the Biot coefficient and stresses are defined positive in tension and the pressure of the solid positive in compression. The pressure of the solid phase follows from

$$p_s = p_g - \chi (p_g - p_w) \quad (18)$$

and takes into account the pressure p_w of the pore water and in case of partially saturation the gas pressure p_g . The Bishop parameter χ is a function of saturation controls the influence of the fluid pressure on the effective stress. Here, χ is defined by $\chi = S_w$ as proposed in Lewis *et al.* (1998).

The effective stress controls the mechanical behavior, thus all material models for the description of the deformation behavior of concrete have to be defined employing effective stresses.

4.3.2 Material model

The mathematical description of the mechanical behavior of the aging concrete is achieved by a set of ordinary differential equations of first order with respect to time. The current state of the aging material is described by internal variables and evolution equations.

The mechanical properties of concrete are not constant during the life cycle and firstly develop during the hydration process. Parameter like elastic modulus and tensile strength depends on the degree of hydration m , which is considered by

$$\frac{P_{(m),i}}{P_{\infty,i}} = \left(\frac{m - m_0}{m_{\infty} - m_0} \right)^{\alpha_i} \quad (19)$$

where $P_{(m),i}$ is the material parameter, which depends on the hydration process, $P_{\infty,i}$ the final value and α_i an additional progression parameter. Furthermore m_0 defines the start point of the development.

In general, the total strain rate in concrete may be split under the assumption of small deformations into the components

$$\dot{\boldsymbol{\varepsilon}} = \dot{\boldsymbol{\varepsilon}}_{el} + \dot{\boldsymbol{\varepsilon}}_{pl} + \dot{\boldsymbol{\varepsilon}}_{th} + \dot{\boldsymbol{\varepsilon}}_{sh} + \dot{\boldsymbol{\varepsilon}}_{cr}. \quad (20)$$

The elastic strain rate is defined by

$$\dot{\boldsymbol{\varepsilon}}_{el} = \frac{\partial}{\partial t} (\mathbf{F} \boldsymbol{\sigma}) \quad (21)$$

where \mathbf{F} is the flexibility matrix, which includes the hardening of the material during hydration as well as the softening. The unit volume expansion $\boldsymbol{\varepsilon}_{th}$ depends on temperature and the thermal expansion coefficient. The shrinkage strains are defined with

$$\dot{\boldsymbol{\varepsilon}}_{sh} = \frac{\partial}{\partial t} \left(\frac{\alpha}{3K_T} p_s \right) \mathbf{I} \quad (22)$$

and depend on the pressure of the solid phase p_s , the Biot coefficient α and the bulk modulus of the matrix K_T . In this work, the shrinkage strains are taken into account indirectly via the concept of effective stresses. Thus, they have not to be considered additionally in the strain balance.

The creep strains and the plastic strains are formulated within the framework of visco-plasticity considering mechanical damage. Here, the creep strains are splitted into two parts, the basic creep and the long term creep, which called drying creep. The basic creep is modeled by means of the solidification theory proposed by Bažant *et al.* (1989). The long term creep or drying creep is described by the microprestress theory, which was introduced by Bažant *et al.* (1997) and applied to multiphase porous material like concrete by Gawin *et al.* (2006).

Due to the framework of visco-plasticity the stress state at a material point is bounded by a failure surface consisting of a Rankine criterion (index R) for tensile principal stresses and of a Drucker-Prager criterion (index DP) for compressive stresses. Using Koiter's flow rule for multi-surface plasticity, the plastic strains for stress states at the surface are defined by

$$\dot{\boldsymbol{\varepsilon}}_{pl} = \sum_k^{n_f} \dot{\lambda}_k \frac{\partial F_k}{\partial \boldsymbol{\sigma}} \quad \text{with } n_f = R, DP. \quad (23)$$

The combination of visco-plasticity and mechanical damage is realized successfully by using the effective stress tensor $\tilde{\boldsymbol{\sigma}}$. In this work the principle of energy equivalence is taken into account, which considers stresses, strains, elasticity and flexibility matrix as affected by damage.

The evolution of the local isotropic damage of each failure surface bases on an exponential approach by Peerling *et al.* (1998). The total mechanical damage is defined as a product of damage

in tension and compression by

$$D_{mech} = 1 - (1 - D_R) \cdot (1 - D_{DP}). \quad (24)$$

The proposed damage formulation of Eq. (24) leads to energy dissipation, inelastic effects and high strain gradients, which accumulate in areas called process zones. Therefore a non-local model developed by Engelen *et al.* (2003) is used for determination of the two nonlocal inelastic proportionality factors, which are defined by

$$\begin{aligned} \bar{\lambda}_{DP} - l_c^2 \nabla^2 \bar{\lambda}_{DP} &= \lambda_{DP}, \\ \bar{\lambda}_R - l_c^2 \nabla^2 \bar{\lambda}_R &= \lambda_R. \end{aligned} \quad (25)$$

The dimension of the damage process zone is developed by an additional material parameter called characteristic length l_c , which is estimated as equal in compression and tension.

5. Solution algorithm

The material models of Section 4 are introduced into the balance equations of Section 3. The nonlinear and coupled set of equations is solved in a monolithic algorithm in the framework of the finite element method, which is presented in the following.

The first step of the solution procedure is the definition of the primary variables. Here, the displacements \mathbf{u} , the nonlocal variables $\bar{\lambda}_{DP}$, $\bar{\lambda}_R$, the relative humidity φ , the temperature T , the dry air pressure p_a , the concentration of salt in the solution $\omega_{\gamma w}$ and the concentration of carbon dioxide in the dry air $\omega_{\kappa a}$ are chosen, which are combined to

$$\mathbf{z}^T = [\mathbf{u}, \bar{\lambda}_{DP}, \bar{\lambda}_R, \varphi, T, p_a, \omega_{\gamma w}, \omega_{\kappa a}]. \quad (26)$$

In the second step the initial values $\mathbf{z}_{t=0} = \bar{\mathbf{z}}_0$ and the boundary values have to be defined. The default initial values of this paper are presented in Table 1. Boundary conditions of Dirichlet type, Neumann type and Cauchy type may be used in the following simulations. Thereby, the boundary conditions of the mass and the energy balances are registered only with conditions of Cauchy type.

Table 1 Initial values

variable	\mathbf{u}	$\bar{\lambda}_{DP}, \bar{\lambda}_R$	φ	T	p_a	$\omega_{\gamma w}$	$\omega_{\kappa a}$
unit	m	-	%	K	Pa	kg _{salt} /kg _{sol}	kgCO ₂ /kg _{dry air}
value	0	0	99.98	293.15	101325	0	0

With the set of primary variables, including Eq. (26) and the two additional non-local variables, the equations are transferred into the weak form by means of the Galerkin method and discretized by the finite element method. The discretized form of the model equations reads as the non-linear coupled equations

$$\mathbf{C}(\hat{\mathbf{z}}) \frac{\partial \hat{\mathbf{z}}}{\partial t} + \mathbf{K}(\hat{\mathbf{z}}) \hat{\mathbf{z}} = \mathbf{F} \quad (27)$$

with

$$\hat{\mathbf{z}}^T = \left[\hat{\mathbf{u}}, \hat{\lambda}_{DP}, \hat{\lambda}_R, \hat{\varphi}, \hat{\mathbf{T}}, \hat{\mathbf{p}}_a, \hat{\mathbf{w}}_w^\gamma, \hat{\mathbf{w}}_a^\kappa \right]. \quad (28)$$

For the discretization in time an implicit Euler scheme is applied. The system of non-linear equations is solved by the Newton-Raphson procedure.

6. Structural analysis

The application and the capabilities of the proposed model is shown in two following examples. The aim of the simulation is to carry out the importance of considering aging effect by taken into account the load history of the structure into the simulations. A neglect of aging effects leads to an overestimation of the resistance and the durability of the structure.

6.1 First example

In the first example a slab with a thickness of 30 cm is investigated. Due to the dimension of the slab transport processes proceed only in direction of the thickness. The assumption of the same boundary conditions on the top and the bottom of the slab leads to a symmetric system, which is taken into account, see Fig. 3. All displacements are disabled in longitudinal direction, thereby imposed deformation due to shrinkage or thermal strains are possible. The composition of the concrete corresponds to the mixture, which is experimental investigated by Bentz *et al.* (1998). All mechanical and transport parameters are given in Table 2.

The simulation starts with the hydration process at $t = 0$ h. Therefore the necessary principle variables displacement, relative humidity, temperature and pressure of dry air are selected and the corresponding principle processes and material models are activated.

Within the first 48 h of the hardening process, the concrete is being protected against desiccation and only a convective heat transport with an outer temperature $T_\infty = 20^\circ\text{C}$ is considered. After two days under sealed conditions the young concrete is exposed to ambient conditions with $T_\infty = 20^\circ\text{C}$ and $\varphi_\infty = 60\%$ over a period of 50 days. Fig. 4 show the results over the depth for $t = 50$ d.

After 50 days the hydration process is almost fully completed and the degree of hydration reached the final value inside the slab. Only in areas near to the surface the degree of hydration is less then m_∞ because φ_∞ of the ambiance leads to a drying and reduction of the relative humidity, see Fig. 4(a).

Due to the high w/c ratio of the concrete composition the hydration reaction leads only to a low reduction of the saturation inside the slab. Against this, the drying process causes a sharp decrease of saturation in the outer layers. Furthermore the drying leads to a deformation of the structure, the so-called drying shrinkage. However the selected boundary conditions prevent all deformations in longitudinal direction. Therefore the shrinkage strains cause mechanical damage in areas near to the surface, which is shown in Fig. 4(b). During the hydration reaction the porosity of the cement paste is decreasing. Therefore, the incomplete hydration process in areas near to the surface involves a higher porosity, see Fig. 4(a).

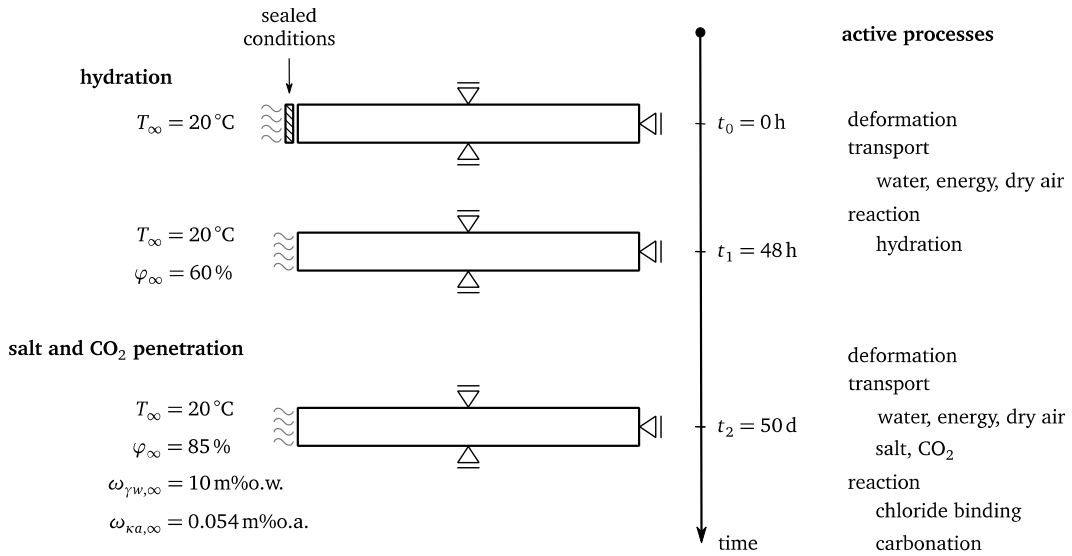
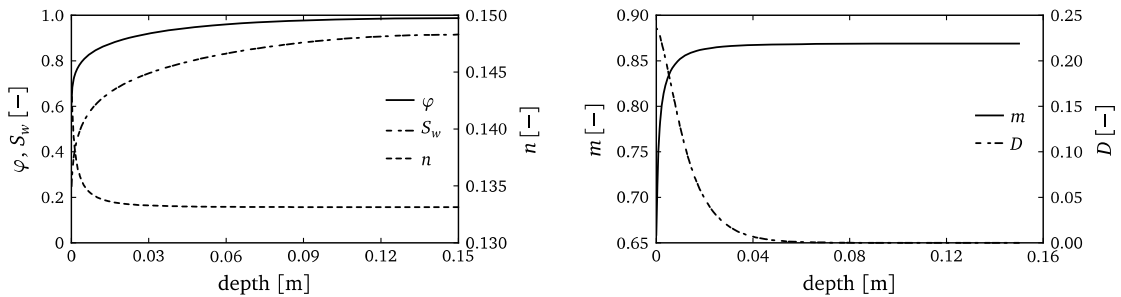


Fig. 3 Boundary conditions and active processes for first example

Table 2 Material parameter

<i>composition</i>	<i>mechanical</i>	<i>transport</i>
$c = 275 \text{ kg/m}^3$	$E = 30000 \text{ MN/m}^2$	$k\theta = 8 \times 10^{-21} \text{ m}^2$
$w = 179 \text{ kg/m}^3$	$\nu = 0.2$	$D_g^V = 2.5 \times 10^{-5} \text{ m}^2/\text{s}$
$\rho_c = 2188 \text{ kg/m}^3$	$f_c = 30 \text{ MN/m}^2$	$D_g^K = 1.5 \times 10^{-5} \text{ m}^2/\text{s}$
$m_\infty = 0.87$	$f_t = 3.0 \text{ MN/m}^2$	$D_W^\gamma = 8.3 \times 10^{-10} \text{ m}^2/\text{s}$



(a) Relative humidity, saturation and porosity

(b) Degree of hydration and mechanical damage

Fig. 4 Results of the hydration process of first example after 50 days

The results of the hydration process serve under the assumption of a terminated hydration process as initial values for the following simulation of the salt and carbon dioxide penetration, which starts after 50 days. The relevant boundary conditions are given in Fig. 3. The concrete is exposed to a 10% salt solution for 2 years. Additionally the carbon dioxide concentration of the atmosphere is considered. However, the carbonation process is not relevant in such a short observation period.

To evaluate the influence of coupling the hydration and chloride penetration process, a standard chloride penetration simulation is carried out assuming a homogenous distribution of material parameters and a constant temperature and moisture field of $T_\infty = 20^\circ\text{C}$ and $\varphi_\infty = 60\%$. In the following this simulation is called *case A*, the coupled hydration and chloride penetration simulation *case B*. The results of the free chloride distribution in the cross section for the two cases are presented in Fig. 5(a) after one and two years chloride effect from the ambience. Here, the free chloride content is given in m-% of the cement content.

The results in Fig. 5(a) show a higher free chloride concentration for *case B* as for *case A* at every point in the two time steps. For example, the free chloride concentration for *case B* in a depth of 2 cm from the outer surface is almost three times higher as for *case A*. This results e.g., from the higher porosity and the mechanical damage in areas near to the surface, which lead to a higher permeability and diffusion coefficient and therewith a higher transport velocity. Finally, in *case B* the critical chloride concentration of the concrete, above corrosion of the reinforcement may start, is much faster exceeded. The results show that a disregarding of the aging of the material parameters, in this case the hydration process, leads to an underestimation of the corrosion risk.

Fig. 5(b) shows different modifications of the simulation *case B*. The results allow evaluating the various influences of the effects hydration process, porosity, chloride binding and mechanical damage on the chloride penetration.

The variant *case B-1* takes into account additional to the standard simulation the decrease in porosity due to the chloride binding process with $A_n^{Cl} = -0.1$, see Eq. (11). The reduction of the porosity, which starts at the outer surface, leads to slower transport velocities and therewith a higher chloride concentration in areas near to the surface. However, the differences between *case B* and *B-1* are negligible small.

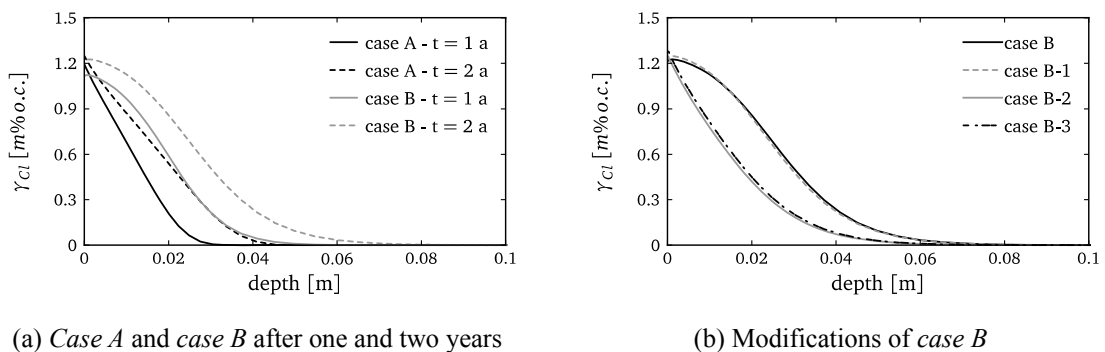


Fig. 5 Results of free chloride content for two cases – A) using only the chloride model with homogenous material parameter as initial conditions - B) coupling hydration and chloride penetration process

In *case B-2* the effect of the mechanical damage is excluded in Eqs. (14) and (16). The transport velocities of the undamaged material is smaller and the chloride concentration inside is lower as in *case B*. Variant *B-3* considers additionally to *B-2* a optimal hydration process with the final degree of hydration in every point. The difference between *B-2* and *B-3* are due to changes in porosity and saturation, but they are very small. In summary, the porosity and the mechanical damage have the most influence on the depth of the chloride penetration.

6.2 Second example

In the second example a column on a slab is investigated. The structure is attacked by a salt solution, which may lead to corrosion of the reinforcement. This is e.g., a typically case of damage in parking garages. In the simulation the hydration and the chloride penetration process of a structure as well as the different concreting times of the slab and the column are observed. The dimension of the slab is 1 x 1 m and the cross section of the column is 40 x 32 cm, therefore the symmetry of the geometry is taken into account. The slab is supported in both longitudinal directions and in vertical direction on the bottom side. Additionally the convective heat transport between the bottom of the slab and the soil is considered with $T_{\infty} = 15^{\circ}\text{C}$, which is constant during the whole simulation. The same material and model parameter as in the previous example are used.

The simulation starts at $t = 0$ h with the hydration process of the slab. During the first 24 h sealed conditions are considered on the top of the slab with $T_{\infty} = 20^{\circ}\text{C}$. After one day the slab is exposed to ambient conditions with $\varphi_{\infty} = 60\%$ at the same temperature. The casting of the concrete column occurs after 20 days and the hardening starts under sealed conditions. After further two days the formwork is stripped from the column and ambient conditions are considered for the column, too.

The results of the hydration process are shown in Figs. 7 and 8 after 100 days. Fig. 7(a) depicts the degree of hydration m . Inside the structure m achieved nearly the final value m_{∞} . Against this the drying effect of the ambience stopped the hydration process in areas near to the surface and causes $m < m_{\infty}$.

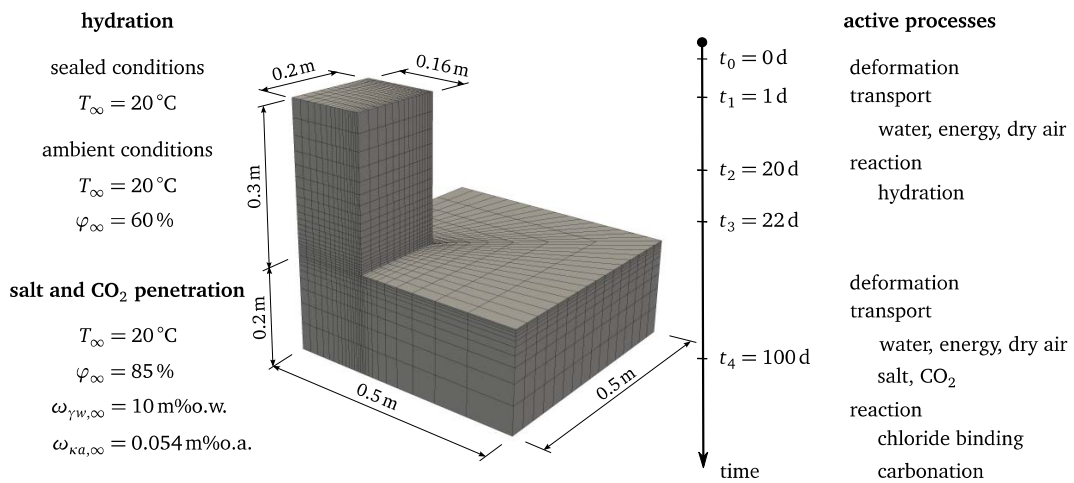


Fig. 6 Boundary conditions and active processes for second example

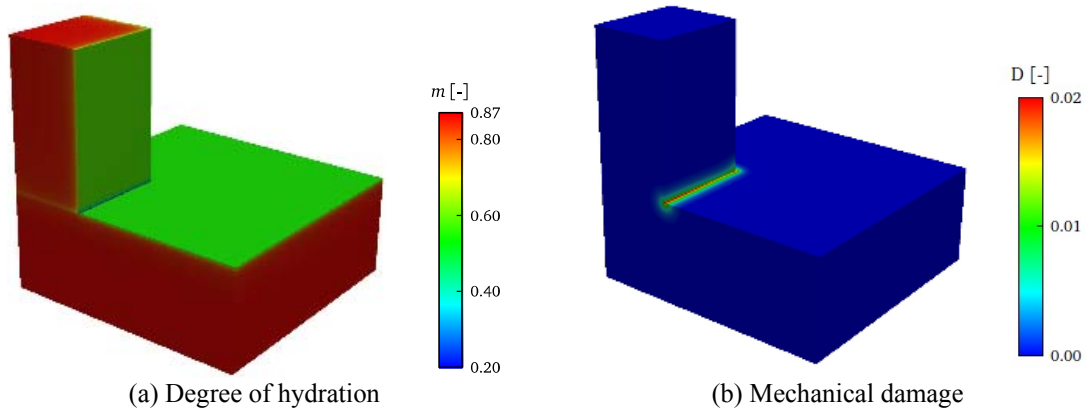


Fig. 7 Results of the hydration process of second example after 100 days

Between the slab and the column, the degree of hydration is smaller than m_∞ , too. This results from the successively concreting of slab and column. Before casting the column, drying leads to a decrease of the saturation in the top of the slab. In the first time after concreting the column, the saturation gradient between slab and column causes a water transport from the column into the slab. The reduced water content in the column leads to a decrease of the reaction rate of the hydration process and therefore $m < m_\infty$.

The results of the mechanical damage are shown in Fig. 7(b). On the one hand, the damage results from the boundary conditions of the formwork for the concreting of the column. On the other hand, the damage occurs because of differences in material properties due to the different age of the slab and the column. Finally, the continuing drying leads to additional shrinkage and mechanical damage.

The contour plot of the relative humidity in Fig. 8(a) shows the drying of the outer layers. Additionally the results indicate differences between the relative humidity on the top of the slab and the surface of the column. This is due two main reasons. Firstly, the soil cools the slab because of its lower temperature. Secondly, the boundary conditions of the water balance is set via a Cauchy boundary conditions for the vapor pressure with a constant vapor pressure of the ambience. Therefore, the difference in temperature between slab and column causes the difference in relative humidity.

Fig. 8(b) shows the water saturation of the material after 100 days. The results indicate a lower saturation in the joint between the slab and the column. But the corresponding relative humidity shows a uniform course. The reason for this is that the lower degree of hydration in this area affects the saturation function and leads to a lower saturation for the same relative humidity level in the joint, see Eq. (12).

Under the assumption of an ended hydration process after 100 days the results are applied as initial values for the second part, the chloride penetration. The outer surfaces of the column and the top of the slab are exposed to a relative humidity and a salt solution of $\varphi_\infty = 85\%$ and 10% . All boundary conditions are constant during the simulations.

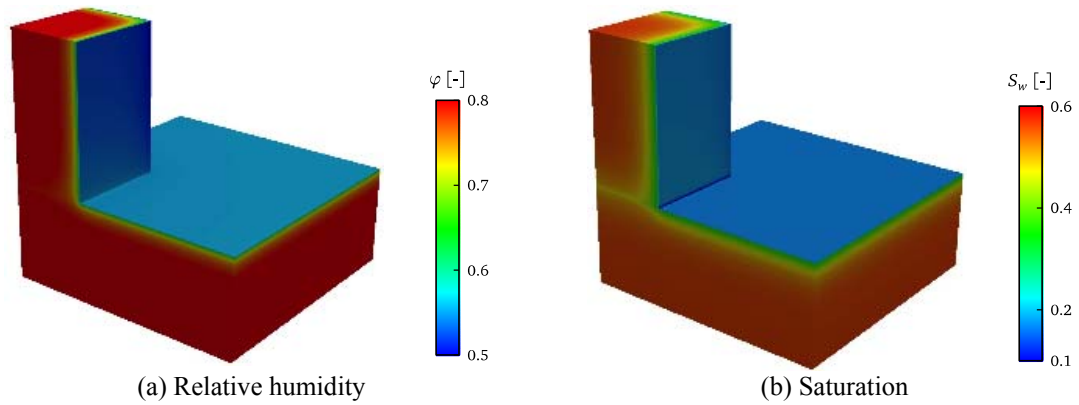


Fig. 8 Relative humidity and saturation after 100 days

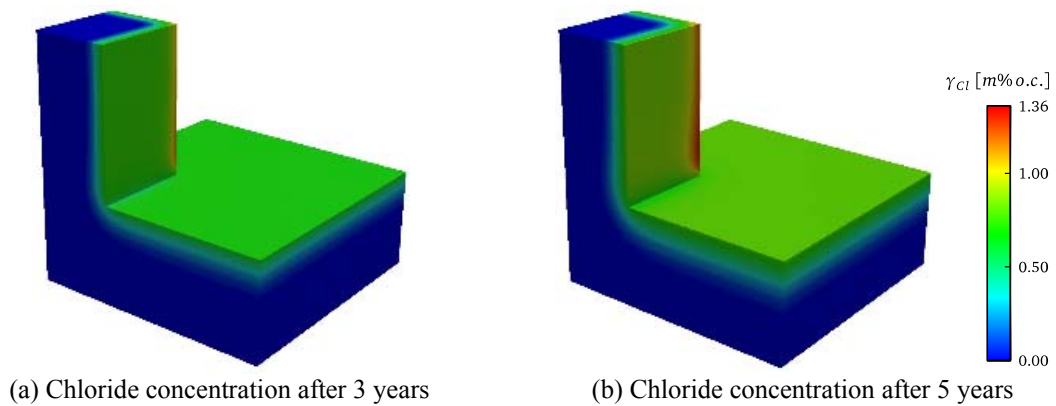


Fig. 9 Free chloride concentration after 3 and 5 years

The contour plots of Figs. 9(a) and 9(b) show the results for the free chloride concentration after 3 and 5 years. The chloride penetration starts at the outer surface. After the observed period the highest chloride content exists in the corner with about 1.36 m-% o.c.

The chloride poses not directly a risk for the concrete. However, when the chloride content at the reinforcement exceeds a critical chloride content, corrosion may occur, if additionally conditions are fulfilled. This corrosion process is often called chloride-induced corrosion and leads to decrease of resistance of the reinforcement and to a damage of the surrounding concrete due to volume growth of the reaction products. The critical chloride content is defined differently in the literature. Here, the critical chloride content of the free chloride is set to 0.6 m-% o.c. which corresponds to 0.3 m-% o.c. for the free chloride content, see Gehlen (2000) and Steffens (2000).

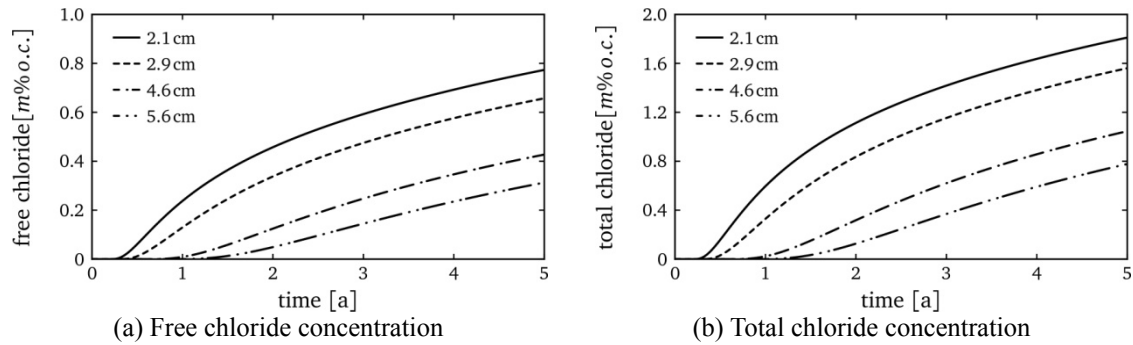


Fig. 10 Results for free and total chloride concentration

Figs. 10(a) and 10(b) show the temporal changes of the free and total chloride content of four points in the corner of the column, which lie in different distance to the outer surface. All points are in a plane 2 cm above the bottom of the column. The results shows, that the critical chloride content is exceeded in a depth of 2.1 cm after 1 year. In a depth of 5.6 cm the critical chloride content is passed after 4 years. The short time of exceeding the critical value is due to two main reasons. One the hand, the used mixture with the high w/c-ratio and the corresponding high porosity has only low durability properties. On the other hand, the high external chloride concentration, which is also constant over time, does not comply with real situation. For example the salt concentration in the North Sea is about 3.5%. But the results show, that the model allows to combine different processes and to take into account aging effects from previous processes.

7. Conclusions

The presented model allows the description of the most important aging processes in concrete in order to predict the durability of concrete structures during their life cycle. Although a single consideration as well as a coupling of different processes is possible. An overview of the design of the theoretical model is given and the balance equations for linear momentum, mass and energy as well as additional material models for the stress-strain relationship, the transport behavior and the chemical reactions are explained. Finally, the results of two numerical durability analyses of concrete structures are discussed.

Applications of the model to durability analysis of concrete under chloride and carbonate attack indicate, that the consideration of the load history and therefore changes in material structure and material parameters influences strongly the depth of chloride penetration. Excluding these aging effects leads to an overestimation of material capabilities. Thus the presented numerical model allows a more detailed and realistic description of aging processes in concrete structures during their life cycle.

References

- Bangert, F., Kuhl, D. and Meschke, G. (2004), "Chemo-hygro-mechanical modelling and numerical simulation of concrete deterioration caused by alkali-silica reaction", *Int. J. Numer. Anal. Meth. Geomech.*, **28**(7-8), 689-714.
- Baroghel-Bouny, V., Mainguy, M., Lassabatere, T. and Coussy, O. (1999), "Characterization and identification of equilibrium and transfer moisture properties for ordinary and high-performance cementitious materials", *Cement Concrete Res.*, **29**(8), 1225-1238.
- Baroghel-Bouny, V., Thiéry, M. and Wang, X. (2011), "Easy assessment of durability indicators for service life prediction or quality control of concretes with high volumes of supplementary cementitious materials", *Cement Concrete Res.*, **33**(8), 832-847.
- Bazant, Z.P. and Prasannan, S. (1989), "Solidification theory for concrete creep. I: formulation", *J. Eng. Mech. - ASCE*, **115**(8), 1691-1703.
- Bazant, Z.P., Hauggaard, A.B., Baweja, S. and Ulm, F.J. (1997), "Microprestress-solidification theory for concrete creep. I: Aging and drying effects", *J. Eng. Mech. - ASCE*, **123**(11), 1188-1194.
- Bentz, D.P., Waller, V. and de Larrard, F. (1998), "Prediction of adiabatic temperature rise in conventional and high-performance concretes using a 3-D microstructural model", *Cement Concrete Res.*, **28**(2), 285-297.
- Derluyn, H., Moonen, P. and Carmeliet, J. (2014), "Deformation and damage due to drying-induced salt crystallization in porous limestone", *J. Mech. Phys. Solids*, **63**, 242-255.
- Engelen, R.A.B., Geers, M.G.D. and Baaijens, F. (2003), "Nonlocal implicit gradient-enhanced elasto-plasticity for the modelling of softening behaviour", *Int. J. Plasticity*, **19**(4), 403-433.
- Gawin, D., Pesavento, F. and Schrefler, B.A. (2003), "Modelling of hygro-thermal behaviour of concrete at high temperature with thermo-chemical and mechanical material degradation", *Comput. Method. Appl. M.*, **192**(13-14), 1731-1771.
- Gawin, D., Pesavento, F. and Schrefler, B.A. (2006), "Hygro-thermo-chemo-mechanical modelling of concrete at early ages and beyond. Part II: shrinkage and creep of concrete", *Int. J. Numer. Meth. Eng.*, **67**(3), 299-331.
- Gehlen, C. (2000), "Probability-based service life design of reinforced concrete structures. Reliability studies for prevention of reinforcement corrosion", *Deutscher Ausschuss für Stahlbeton*, (510), (in German).
- Jensen, O.M. and Hansen, P.F. (2001), "Water-entrained cement-based materials: I. principles and theoretical background", *Cement Concrete Res.*, **31** (4), 647-654.
- Lewis, R. and Schrefler, B.A. (1998), *The finite element method in the static and dynamic deformation and consolidation of porous media*, John Wiley & Sons.
- Ostermann, L. (2011), *Hochtemperaturverhalten von Beton - Gekoppelte Mehrfeld-Modellierung und numerische Analyse*, Ph.D. Dissertation, TU Braunschweig, Braunschweig.
- Pantazopoulou, S.J. and Mills, R.H. (1995), "Microstructural aspects of the mechanical response of plain concrete", *ACI Mater. J.*, **92**(6), 605-616.
- Peerlings, R.H.J., De Borst, R., Brekelmans, W.A.M. and Geers, M.G.D. (1995), "Gradient-enhanced damage modelling of concrete", *Mech. Cohesive-Frictional Mater.*, **3**(4), 323-342.
- Saetta, A.V., Schrefler, B.A. and Vitaliani, R.V. (1993), "The carbonation of concrete and the mechanism of moisture, heat and carbon dioxide flow through porous materials", *Cement Concrete Res.*, **23**(4), 761-772.
- Steffens, A. (2000), *Modellierung von Karbonatisierung und Chloridbildung zur numerischen Analyse der Korrosionsgefährdung der Betonbewehrung*, Ph.D. Dissertation, TU Braunschweig, Braunschweig.
- Steffens, A., Dinkler, D. and Ahrens, H. (2002), "Modeling carbonation for corrosion risk prediction of concrete structures", *Cement Concrete Res.*, **32**(6), 935-941.
- Tacke, R. (2002), *Feuchte- und Festigkeitsentwicklung hydratisierenden Betons - Modellierung und numerische Analyse*, Ph.D. Dissertation, TU Braunschweig, Braunschweig.